ACS APPLIED MATERIALS & INTERFACES

Research Article

www.acsami.org

Nanoscaled Poly(L-glutamic acid)/Doxorubicin-Amphiphile Complex as pH-responsive Drug Delivery System for Effective Treatment of Nonsmall Cell Lung Cancer

Mingqiang Li,[†,‡,§] Wantong Song,[†,‡,§] Zhaohui Tang,[‡] Shixian Lv,[‡,§] Lin Lin,[‡] Hai Sun,[‡] Quanshun Li,[‡] Yan Yang,[‡] Hua Hong,*[,⊥] and Xuesi Chen*[,‡]

[‡] Key Laboratory of Polymer Ecomaterials, Changchun Institute of Applied Chemistry, Chinese Academy of Sciences, Changchun 130022, P. R. China

[§]University of Chinese Academy of Sciences, Beijing 100039, P. R. China

[⊥]Laboratory Animal Center, Jilin University, Changchun, 130012, P. R. China

Supporting Information

ABSTRACT: Nonsmall cell lung cancer (NSCLC) is the leading cause of cancer-related death worldwide. Herein, we develop a polypeptide-based block ionomer complex formed by anionic methoxy poly(ethylene glycol)-*b*-poly(L-glutamic acid) (mPEG-*b*-PLG) and cationic anticancer drug doxorubicin hydrochloride (DOX·HCl) for NSCLC treatment. This complex spontaneously self-assembled into spherical nanoparticles (NPs) in aqueous solutions via electrostatic interaction and hydrophobic stack, with a high loading efficiency (almost 100%) and negative surface charge. DOX·HCl release from the drug-loaded micellar nanoparticles (mPEG-*b*-PLG-DOX·HCl) was slow at physiological pH, but obviously increased at the acidic pH mimicking the endosomal/lysosomal environment. In vitro cytotoxicity and hemolysis assays demonstrated that the block copolypeptide was cytocompatible and hemocompatible, and the presence of copolypeptide carrier could reduce the hemolysis ratio of DOX·HCl significantly. Cellular uptake and cytotoxicity studies suggested that mPEG-*b*-PLG-DOX·HCl was taken up by A549 cells via endocytosis, with a slightly slower cellular internalization and lower cytotoxicity compared with free DOX·HCl. The pharmacokinetics study in rats showed that DOX·HCl-loaded micellar NPs significantly prolonged the blood circulation time. Moreover, mPEG-*b*-PLG-DOX·HCl exhibited enhanced therapeutic efficacy, increased apoptosis in tumor tissues, and reduced systemic toxicity in nude mice bearing A549 lung cancer xenograft compared with free DOX·HCl, which were further confirmed by histological and immunohistochemical analyses. The results demonstrated that mPEG-*b*-PLG was a promising vector to deliver DOX·HCl into tumors and achieve improved pharmacokinetics, biodistribution and efficacy of DOX·HCl with reduced toxicity. These features strongly supported the interest of developing mPEG-*b*-PLG-DOX·HCl as a valid therapeutic modality in the therapy of human NSCLC and other solid tumors.

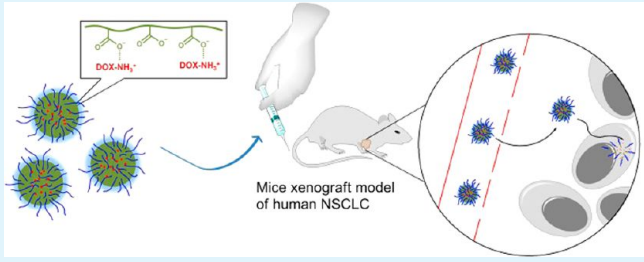

KEYWORDS: *poly(L-glutamic acid), doxorubicin hydrochloride, electrostatic interaction, pH-responsive, nonsmall cell lung cancer, antitumor*

INTRODUCTION

Lung cancer, one of the most common cancers, is the leading cause of cancer-related morbidity and mortality, resulting in approximately one-third of all cancer-related deaths worldwide.[1] Nonsmall cell lung cancer (NSCLC) accounts for about 80% of all lung cancers.[2] Conventional modalities, such as surgical resection, radiotherapy, chemotherapy, or their combinations, are conceived as the primary treatment choices for NSCLC. Unfortunately, it is difficult to remove tumor tissue completely in most cases. Even worse, more than 70% of patients with lung cancer present with locally advanced or metastatic disease at the time of diagnosis, resulting in a dismal 5-year survival rate of less than 16%,[3] which highlights the urgent need for more effective therapeutic strategies.

Doxorubicin hydrochloride (DOX·HCl), an anthracycline antibiotic, is the first line treatment used for a wide range of cancers. However, the dose-dependent cardiotoxicity, myelosuppression, nephrotoxicity, and development of multidrug resistance associated with unformulated DOX·HCl limit its therapeutic efficacy.[4] Many new and innovative strategies to entrap DOX·HCl in different nanocarriers with a variety of architectures including polymer-drug conjugates, micelles, nanogels, liposomes, dendrimers, and nanospheres have been developed to overcome this limitation.

Received: December 11, 2012
Accepted: February 14, 2013
Published: February 14, 2013

dx.doi.org/10.1021/am303073u | ACS Appl. Mater. Interfaces 2013, 5, 1781−1792

Amphiphilic polypeptide-based block copolymers have attracted considerable attention because of their biocompatibility, biodegradability, and precise secondary conformations, making them highly desirable for anticancer drug delivery.[5] Generally, polypeptide amphiphiles consist of poly(ethylene glycol) (PEG) and hydrophobically derivatized polypeptide blocks. The hydrophobic core serves as either a reservoir within which hydrophobic drugs (e.g., paclitaxel,[6] doxorubicin,[7] and amphotericin B[8]) are encapsulated, or the drugs (e.g., paclitaxel,[9] doxorubicin,[10,11] and SN 38[12]) are covalently bound to the polymer. In addition to encapsulate hydrophobic drugs within the interior core of these amphiphilic polymeric micelles, ionic block polymers with good water solubility may also self-assemble into core−shell nanostructures when loaded with oppositely charged components (e.g., lysozyme[13] and DNA[14]) or platinum(II) antitumor drugs.[15,16] This is achieved by exploiting the electrostatic or chelate interactions between the ionic polypeptide block of the polymeric carrier and the biological macromolecular drug or platinum(II) antitumor drugs.

Most of the reported hydrophobic drug encapsulation procedures involve the dissolution of the polymeric carrier and drug in an organic solvent, and the subsequent removal of the organic solvent by either dialysis or solvent evaporation.[17] The use of organic solvents in pharmaceutical formulations is rarely desirable, owing to their potential deleterious effects and the regulatory requirement to quantify residual levels of harmful organic solvents.[5] If possible, the drug encapsulation procedure should avoid using organic solvent to ensure the safe and effective drug-use for patients. A number of stories involving doxorubicin delivery via hydrophobic interaction between the drug and hydrophobic moieties of the drug carrier have been reported in the past few years.[7,18] As a general rule, DOX·HCl was neutralized by excess triethylamine to remove the hydrochloride and make doxorubicin hydrophobic in organic solvents (DMF or DMSO).[19,20] Nevertheless, the trace residual triethylamine and solvent may do harm to the human body. Recently, few attempts have been made to load hydrophilic DOX·HCl, which is a weak amphipathic base (pK_a 8.3), into anionic polymers through electrostatic interaction in aqueous medium.[21−27] However, most of the reported anionic polymer/DOX·HCl complexations were based on nonbiodegradable polymers (e.g., poly(methacrylic acid) and poly(acrylic acid)) and devoid of in vivo studies.[22−27]

Another major concern in pharmaceutical industry consists in establishing convenient and reproducible methods to achieve high loading content (LC) and loading efficiency (LE).[27] In this aim, DOX·HCl is usually loaded into the aqueous interior of preformed vesicles by applying ionic or pH gradients across the liposome or polymersome bilayer.[25,28] On the other hand, anionic polymers such as γ-polyglutamic acid can also specifically interacts with cationic DOX·HCl via electrostatic interaction forming random colloidal aggregates and results in almost 100% complexation efficiency.[26] Despite of such high association, these DOX·HCl loaded complexes exhibit negative zeta potential, which may reduce the undesirable clearance by the reticuloendothelial system (RES) such as liver, to improve the blood compatibility and deliver the drug more efficiently to the tumor sites.[29] Yet, it is worthy to note that these anionic polymer/DOX·HCl complexes are relatively stable at neutral pH but dissociate slowly under lower pH analogous to the acidic environment in endosome/lysosome, suggesting that the DOX·HCl-loaded nanocomposites may be suitable for intracellular drug delivery.[22,26,30]

Here, we describe a polypeptide-based delivery system loaded with cationic DOX·HCl via electrostatic interaction and intermolecular hydrophobic stack for the treatment of NSCLC. The DOX·HCl-loaded methoxy poly(ethylene glycol)-*b*-poly(L-glutamic acid) (mPEG-*b*-PLG-DOX·HCl) was evaluated for physicochemical properties, release profile, cellular uptake, in vitro cytotoxicity, hemolytic activity, pharmacokinetics, tissue distribution, and in vivo antitumor efficacy. This DOX·HCl-loaded amphiphilic ionic complex showed reduced systemic toxicity, relatively long blood circulation, and enhanced antitumor efficacy compared with free DOX·HCl, indicating a potential utility of the micellar formulation incorporating DOX·HCl in the treatment of NSCLC and other solid tumors.

MATERIALS AND METHODS

Materials. Poly(ethylene glycol) monomethyl ether (mPEG, M_n = 5000) and 2,2′-(ethylenedioxy) bis (ethylamine) were purchased from Aldrich and used without further purification. The amino group terminated poly(ethylene glycol) monomethyl ether (mPEG-NH_2) and γ-benzyl-L-glutamate-N-carboxyanhydride (BLG-NCA) were synthesized as described in our previous works.[31] Doxorubicin hydrochloride (DOX·HCl) was purchased from Beijing Huafeng United Technology Corporation. 3-(4,5-Dimethyl-thiazol-2-yl)-2,5-diphenyl tetrazolium bromide (MTT) and 4′,6-diamidino-2-phenylindole dihydrochloride (DAPI) were purchased from Sigma and used as received. *N*,*N*′-Dimethylformamide (DMF) was stored over calcium hydride (CaH_2) and purified by vacuum distillation with CaH_2. Clear polystyrene tissue culture treated 6-well and 96-well plates were obtained from Corning Costar. Purified deionized water was prepared by the Milli-Q plus system (Millipore Co., Billerica, MA, USA).

Measurements. ^{1}H NMR spectra were recorded on a Bruker AV 400 NMR spectrometer in CF_3COOD. Number-, weight-average molecular weights (M_n, M_w) and molecular weight distributions (polydispersity index, PDI = M_w/M_n) of mPEG-*b*-PBLG were determined by gel permeation chromatography (GPC) using a series of linear Tskgel Super columns (AW3000 and AW5000) and Water 515 HPLC pump, with OPTILAB DSP Interferometric Refractometer (Wyatt Technology) as the detector. The eluent was DMF containing 0.01 M lithium bromide (LiBr) at a flow rate of 1.0 mL min^{-1} at 50 °C. Monodispersed polystyrene standards were used to generate the calibration curve. GPC analysis of mPEG-*b*-PLG were conducted on a Waters 2414 system equipped with Ultrahydrogel linear column and a Waters 2414 refractive index detector (eluent: 0.1 M phosphate buffer, pH 7.4; flow rate: 1.0 mL min^{-1}; temperature: 35 °C; standard: Poly(ethylene glycol)). Dynamic laser scattering (DLS) measurements were performed on a WyattQELS instrument with a vertically polarized He−Ne laser (DAWN EOS, Wyatt Technology). The scattering angle was fixed at 90°. Transmission electron microscopy (TEM) measurements were performed on a JEOL JEM-1011 transmission electron microscope with an accelerating voltage of 100 KV. Zeta potentials (ζ-potential) of the DOX·HCl-loaded mPEG-*b*-PLG micellar nanoparticles (NPs) were estimated on a Zeta Potential/BI-90Plus particle size analyzer (Brookhaven, USA) at 25 °C.

Synthesis of mPEG-*b*-PLG Diblock Copolymer. mPEG-*b*-PLG diblock copolymer was synthesized through ring-opening polymerization of BLG-NCA monomer with mPEG-NH_2 as macroinitiator, and then deprotection of benzyl groups according to the literature procedure.[32] Typically, BLG-NCA (3.951 g, 15.0 mmol) and mPEG-NH_2 (3.0 g, 0.6 mmol) were dissolved in 70 mL of dry DMF in a flame-dry flask. The polymerization was performed at 25 °C for 3 days. Then, the solution was precipitated into excess amount of cold diethyl ether for 3 times to give the methoxy poly(ethylene glycol)-*b*-poly(γ-benzyl-L-glutamate) (mPEG-*b*-PBLG) block copolymers. Subsequently, mPEG-*b*-PBLG (3.890 g) was dissolved in 40 mL of dichloroacetic acid at 25 °C in a flask. After 9 mL of HBr/acetic acid

(33 wt %) was added, the solution was slowly stirred at 30 °C for 1 h and then the final product was precipitated into excessive diethyl ether. After dried under vacuum, the precipitate was dialyzed against distilled water and freeze-dried, yielding a white solid.

Preparation of DOX·HCl-Loaded Micellar NPs. mPEG-*b*-PLG lyophilized powder was dissolved in deionized water and stirred for 10 min, then adjust pH to 7.4 with a few drops of 0.1 M NaOH. DOX·HCl was added into the solution and the mixture solution was vigorously stirred overnight in the dark. Excess drug was removed by dialysis (MWCO 3500) against deionized water for 24 h (The dialysis medium was changed five times) and followed by lyophilization in the dark. For determination of drug loading content (DLC) and loading efficiency, lyophilized drug-loaded polymeric NPs were dissolved in acetonitrile/water (3/7, V/V, pH was adjusted to 3.0 using phosphoric acid) and measured by UV−vis spectrometer at 480 nm. Drug loading content and drug loading efficiency (DLE) were calculated according to the following formula:

$$\text{DLC (wt \%)} = (\text{weight of loaded drug/weight of drug-loaded NPs}) \times 100\%$$

$$\text{DLE (wt \%)} = (\text{weight of loaded drug/weight of feeding drug}) \times 100\%$$

FITC-labeled mPEG-*b*-PLG-DOX·HCl was prepared using a modified version of the method published by Ernsting et al.[33] Briefly, 2,2′-(ethylenedioxy) bis(ethylamine) (9.5 mg, 0.064 mmol) was dissolved in DMSO (2.0 mL), to which FITC (25.0 mg, 0.064 mmol) was added. The solution was stirred for 12 h at room temperature and protected from light. Meanwhile, mPEG-*b*-PLG lyophilized powder (200.0 mg, 0.512 mmol carboxyl groups) was weighed into a glass vial and dissolved in DMSO (5.0 mL), followed by addition of EDC·HCl (25.0 mg, 0.131 mmol) and NHS (7.4 mg, 0.064 mmol). After being stirred overnight at room temperature with protection from light, the amine-modified FITC was covalently linked to mPEG-*b*-PLG with activated carboxylate group by adding FITC solution dropwise to mPEG-*b*-PLG solution. The mixture was stirred for another 24 h at room temperature, and then purified by dialysis for 48 h against deionized water. A light yellow powder was obtained after lyophilization. DOX·HCl was loaded into FITC-labeled mPEG-*b*-PLG by the same procedure used to mPEG-*b*-PLG.

In vitro Release of DOX·HCl. To determine the drug release of DOX·HCl from the NPs of mPEG-*b*-PLG-DOX·HCl, we suspended the weighed freeze-dried DOX·HCl-loaded NPs in 10 mL of release medium and transferred into a dialysis bag (MWCO 3500 Da). The release experiment was initiated by placing the end-sealed dialysis bag into 40 mL of release medium at 37 °C with constant shaking. At selected time intervals, 3 mL release media was taken out and replenished with an equal volume of fresh media. The amount of DOX·HCl released was determined using UV−vis spectrometer at 480 nm.

Cell Culture. The human lung carcinoma (A549), breast cancer (MCF-7) and cervical cancer (Hela) cells were cultured at 37 °C in a 5% CO_2 atmosphere in Dulbecco's modified Eagle's medium (DMEM, Gibco) supplemented with 10% fetal bovine serum (FBS), penicillin (50 U mL^{-1}), and streptomycin (50 U mL^{-1}).

Confocal Laser Scanning Microscopy (CLSM) Observation. The cellular uptake and intracellular release behaviors of DOX·HCl-loaded NPs were determined by CLSM toward A549 cells. The cells were seeded on the coverslip in 6-well plates with a density of 1×10^5 cells per well in 2 mL of DMEM and cultured for 24 h, and then the original medium was replaced with free DOX·HCl and DOX·HCl-loaded NPs (at a final DOX·HCl concentration of 5 mg L^{-1}) containing DMEM. After 1 and 3 h incubation, the cells were washed and fixed with 4% formaldehyde for 20 min at room temperature. The cells were counterstained with 4, 6-diamidino-2-phenylindole (DAPI) for cell nucleus and Alexa Fluor 488 phalloidin (Invitrogen, Carlsbad, CA) for F-actin following the manufacturer's instructions. The cellular localization was visualized under a laser scanning confocal microscope (Olympus FluoView 1000).

The cellular internalization and the accumulation of FITC-labeled polymer NPs were monitored by confocal laser scanning microscopy (Olympus FluoView 1000). Briefly, the cells were seeded on the coverslip in 6-well plates with a density of 1×10^5 cells per well in 2 mL of DMEM and cultured for 24 h, and then the original medium was replaced with DOX·HCl-loaded NPs (at a final DOX·HCl concentration of 5 mg L^{-1}) containing DMEM. After 1 and 3 h incubation at 4 and 37 °C, the cells were washed and fixed with 4% formaldehyde for 20 min at room temperature, and the cell nuclei were stained with DAPI. Finally, the cells were monitored by confocal laser scanning microscopy.

Cellular Uptake Measured by Flow Cytometry. A549 cells were seeded in 6-well plates with a density of 2×10^5 cells per well in 2 mL of DMEM and incubated for 24 h, and then the original medium were replaced with free DOX·HCl and DOX·HCl-loaded NPs (at a final DOX·HCl concentration of 5 mg L^{-1} or 1 mg L^{-1}) containing DMEM. The cells were incubated for 1 and 3 h (or 1, 3, and 24 h) at 37 °C, and then washed three times with PBS. The harvested cells were suspended in PBS and centrifuged at 1000 rpm for 5 min at 4 °C. The supernatants were discarded and the cells were washed with PBS to remove the background fluorescence in the medium. After two cycles of washing and centrifugation, cells were resuspended with 500 μL of PBS, and flow cytometry was done using a BD FACSCalibur flow cytometer from BD Biosciences.

Cytotoxicity Assay. The cytotoxicities of mPEG-*b*-PLG, free DOX·HCl and mPEG-*b*-PLG-DOX·HCl against A549, MCF-7, and Hela cells were evaluated by MTT assay. A549, MCF-7, and Hela cells were seeded in 96-well plates (1×10^4 cells per well) in 100 μL of DMEM medium and incubated at 37 °C in a 5% CO_2 atmosphere for 24 h. The culture mediums were replaced with 200 μL of fresh mediums containing mPEG-*b*-PLG, free DOX·HCl or mPEG-*b*-PLG-DOX·HCl. The cells were subjected to MTT assay after being incubated for another 24 h. The absorbency of the solution was measured on a Bio-Rad 680 microplate reader at 490 nm. The relative cell viability was determined by comparing the absorbance at 490 nm with control wells containing only cell culture medium. Data are presented as means ± SD ($n = 6$).

Cell Apoptosis Analysis. Annexin V-FITC apoptosis detection kit (Keygen Biotech, China) was used to quantify the apoptotic and necrotic cells by a standard fluorescent activated cell sorting (FACS) assay. A549 cells were double stained with Annexin V and PI (propidium iodide), and then subject to flow cytometry (FCM). A549 cells were seeded in 6-well plates with a density of 2×10^5 cells per well in 2 mL of DMEM and incubated for 24 h, and then the original mediums were replaced with free DOX·HCl or DOX·HCl-loaded NPs (at a final DOX·HCl concentration of 1 mg L^{-1}) containing DMEM. After 4 and 24 h incubation, the cells were digested with EDTA-free trypsin, washed twice with cold PBS, and resuspended in binding buffer. Then, the cells were stained with 5 μL of Annexin V-FITC solution and 5 μL of propidium iodide (PI) solution for 15 min at room temperature in the dark. At the end of incubation, 400 μL of binding buffer was added, and the cells were analyzed immediately using flow cytometry.

Hemolysis Assay. Hemolytic activity of mPEG-*b*-PLG, free DOX·HCl, and DOX·HCl-loaded micellar NPs was evaluated according to the previous protocol with minor modification.[34] Briefly, fresh rabbit blood obtained from the Experimental Animal Center of Jilin University was diluted by physiological saline, and then red blood cells (RBCs) were isolated from serum by centrifugation. After carefully washing and diluting, RBC suspension was added to mPEG-*b*-PLG, free DOX·HCl and DOX·HCl-loaded micellar NPs solution at systematically varied concentrations and mixed by vortex, then incubated at 37 °C in a thermostatic water bath for 1.5 h. PBS and triton X-100 (10 g L^{-1}), a surfactant known to lyse RBCs, were used as negative and positive controls, respectively. Then, RBCs were centrifuged at 3000 rpm for 10 min and 100 μL of supernatant of each sample was transferred to a 96-well plate. Free hemoglobin in the supernatant was measured with a Bio-Rad 680 microplate reader at 540 nm. The hemolysis ratio (HR) of RBCs was calculated using the following formula: hemolysis (%) = $(A_{\text{sample}} - A_{\text{negative control}})/(A_{\text{positive control}} - A_{\text{negative control}}) \times 100$, where A_{sample}, $A_{\text{negitive control}}$, and $A_{\text{positive control}}$ were denoted as the absorbencies of samples,

Scheme 1. Schematic Illustration of Drug Loading, Endocytosis, and Intracellular Drug Release of the pH-Responsive Amphiphile Complex

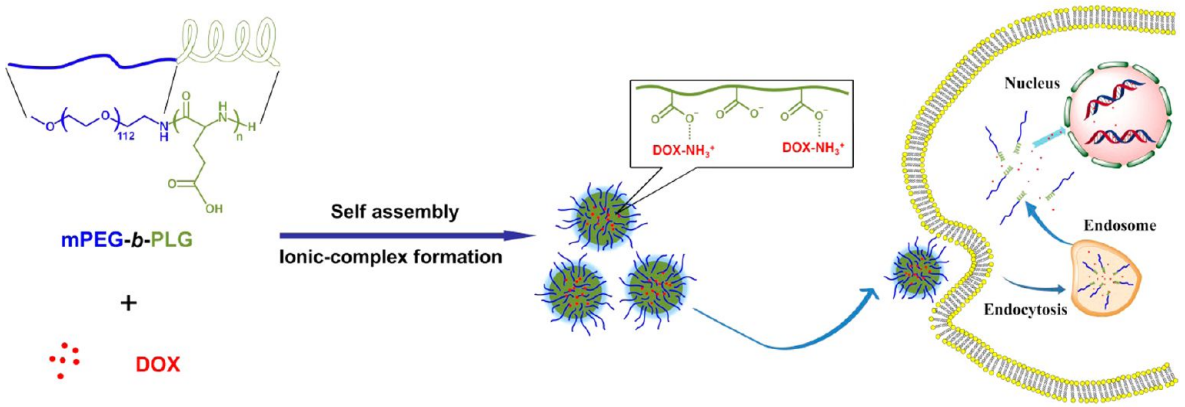

negative and positive controls, respectively. All hemolysis experiments were carried out in triplicates.

Pharmacokinetics. SD rats were randomly divided into two groups (n = 3). Free DOX·HCl and mPEG-*b*-PLG-DOX·HCl were administered intravenous via tail vein (4 mg kg^{-1} on a DOX·HCl basis). At defined time periods (0, 5, 10, 15, 30, 60, 90, 120, 180, 240, 360, 720 min), blood samples were collected from orbital cavity, heparinized, and centrifuged to obtain the plasma. After centrifugation of blood samples, 150 μL aliquots of plasma were stored at −80 °C until HPLC analysis of DOX·HCl.

The concentrations of DOX·HCl in the above samples were determined by the HPLC methods reported previously with slight modifications.[35] A 100 μL plasma sample was deproteinized with 600 μL of acetonitrile and 100 μL of diphenhydramine hydrochloride (5 μg mL^{-1}, internal standard), vortexed for 10 min, and centrifuged at 1200 rpm for 10 min. Then 600 μL of supernatant was collected and dried under a stream of nitrogen at 35 °C. The dried sample was then dissolved in the mobile phase for HPLC analysis. The pharmacokinetic parameters including elimination half-life ($t_{1/2}$), area under the plasma concentration−time curve from zero to the last measurable sample time and to infinity (AUC_{0-t} and $AUC_{0-\infty}$), mean residence time (MRT_{0-t} and $MRT_{0-\infty}$) and clearance rate (CL) were analyzed by noncompartmental analysis using the TopFit 2.0 software package (Thomae GmbH, Germany).

Ex vivo DOX·HCl Fluorescence Imaging. The DOX·HCl-loaded micellar NPs and free DOX·HCl were injected into mice bearing A549 tumor via lateral tail vein (5 mg kg^{-1} on a DOX·HCl basis). The mice were sacrificed 2 and 24 h postinjection. The tumor and major organs (heart, liver, spleen, lung and kidney) were excised, followed by washing the surface with physiological saline three times for ex vivo imaging of DOX·HCl fluorescence using the Maestro in vivo Imaging System (Cambridge Research & Instrumentation, Inc., USA). The resulting data can be used to identify, separate, and remove the contribution of autofluorescence in analyzed images by the commercial software (Maestro 2.4). The average signals were also quantitatively analyzed using Maestro 2.4 software.

In vivo Antitumor Efficiency. Male Balb/C nude mice were obtained from SLRC Laboratory Animal Company (Shanghai, China), and used at 6 weeks of age. All animals received care in compliance with the guidelines outlined in the Guide for the Care and Use of Laboratory Animals and all procedures were approved by the Animal Care and Use Committee of Jilin University.

A human NSCLC xenograft tumor model was generated by subcutaneous injection of A549 cells (1.5×10^6) in the right flank of each mouse. When the tumor volume was approximately 30 − 50 mm^3, mice were randomly divided into 5 groups. Animals were treated with PBS, free DOX·HCl (2 mg kg^{-1}), free DOX·HCl (4 mg kg^{-1}), mPEG-*b*-PLG-DOX·HCl (2 mg kg^{-1} on a DOX·HCl basis) and mPEG-*b*-PLG-DOX·HCl (4 mg kg^{-1} on a DOX·HCl basis) by intravenous injection on days 0, 3, 7, and 10. The tumor size was measured using vernier caliper, and the tumor volume (mm^3) was calculated using $V = ab^2/2$, where a and b were the longest and shortest diameter of the tumors. The body weight was measured simultaneously as an indicator of systemic toxicity. One week after the last treatment, animals were sacrificed and the tumors were excised for histopathology and immunohistochemistry analyses.

Histological and Immunohistochemical Analyses. The mice were sacrificed (one week after the last treatment) and tumors were collected, fixed in 4% PBS buffered paraformaldehyde overnight, and then embedded in paraffin. The paraffin-embedded tumors were cut at 5 μm thickness, and stained with hematoxylin and eosin to assess histological alterations by microscope (Nikon TE2000U).

Immunohistochemistry was performed as described previously.[36,37] Rabbit monoclonal primary antibody for cleaved PARP (Abcam, Cambridge, MA, USA) and PV-6000 two-step immunohistochemistry kit (polymer detection system for immuno-histological staining; Zhongshan Goldbridge Biotechnology, Beijing, China) were used in this study.

In situ terminal Deoxynucleotidyltransferase-Mediated UTP End Labeling (TUNEL) Assay. TUNEL assay was performed using a FragELTM DNA fragment detection kit (colorimetric-TdT Enzyme method) according to the manufacturer's protocol (EMD chemicals Inc., Darmstadt, Germany) with minor modification (In brief, hematoxylin was used as counterstain to replace methyl green).

Statistical Analysis. All experiments were performed at least three times and expressed as means ± SD. Data were analyzed for statistical significance using Student's test. $p < 0.05$ was considered statistically significant, and $p < 0.01$ was considered highly significant.

RESULTS AND DISCUSSION

Preparation of the DOX·HCl-Loaded mPEG-*b*-PLG Micellar NPs. The preparation strategy for DOX·HCl-loaded mPEG-*b*-PLG micellar NPs (mPEG-*b*-PLG-DOX·HCl) was shown in Scheme 1. First, mPEG-*b*-PLG copolymer was prepared (see Scheme S1 in the Supporting Information). Then DOX·HCl was loaded via electrostatic interaction with the carboxylate of the glutamic acid units and intermolecular hydrophobic stack to generate mPEG-*b*-PLG-DOX·HCl.

mPEG-*b*-PLG block copolymer was prepared by the ring-opening polymerization of BLG-NCA using mPEG-NH_2 as the initiator, followed by deprotection of γ-benzyl in HBr/acetic acid.[32,38] The ^{1}H NMR spectra of mPEG-*b*-PBLG and mPEG-*b*-PLG were shown in Figure S1 (in the Supporting Information). The resonances at δ 7.24 and 5.10 ppm disappeared in the mPEG-*b*-PLG, which indicated the complete deprotection of the γ-benzyl groups ($C_6\boldsymbol{H}_5$-, 5H and $C_6H_5C\boldsymbol{H}_2$-, 2H). The degree of polymerization of BLG and

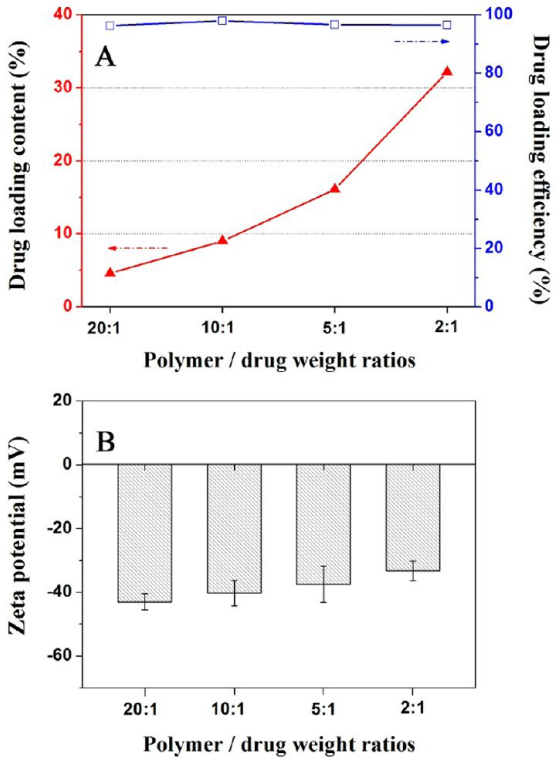

Figure 1. (A) Drug loading content and drug loading efficiency at different weight ratios of polymer to DOX·HCl. (B) Zeta-potential of mPEG-*b*-PLG-DOX·HCl at different weight ratios of polymer to DOX·HCl.

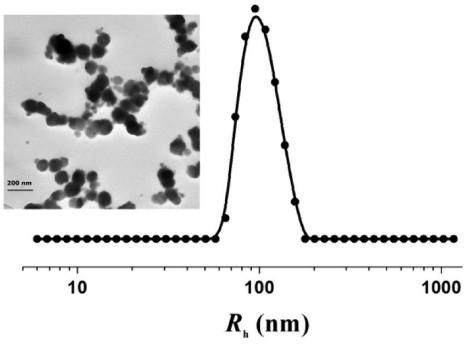

Figure 2. Hydrodynamic radius distribution and morphology of mPEG-*b*-PLG-DOX·HCl in aqueous solution as determined by DLS and TEM.

LG blocks were both calculated to be 20 based on the ratio of integration at peak *e* (−COCH_2-, 2H, PBLG, or PLG block) and peak *b* (-CH_2CH_2O-, 4H, PEG block), suggesting that the deprotection reaction did not result in the scission of poly(glutamic acid) backbones. GPC analyses showed a narrow molecular weight distribution (see Figure S2 in the Supporting Information, mPEG-*b*-PBLG: M_w/M_n = 1.08; Figure S3, mPEG-*b*-PLG: M_w/M_n = 1.07).

DOX·HCl is a positively charged amphiphilic drug, containing protonable amino group in the sugar moiety. DOX·HCl loadings were performed at different feed weight ratios by incubating mPEG-*b*-PLG and DOX·HCl aqueous solutions below its pK_a value, then dialyzing the polymer/drug complex solution to remove unloaded DOX·HCl, and lyophilizing for long-term storage. Drug loading contents and drug loading efficiencies were then determined by spectrophotometry. Almost all of the added DOX·HCl was formed complex with mPEG-*b*-PLG at weight ratio of polymer to drug from 20 to 2, giving the drug loading efficiencies of almost 100% (Figure 1A). We inferred that both the electrostatic interaction between cationic DOX·HCl and anionic carriers, and the hydrophobic stack between DOX·HCl and carriers or DOX·HCl molecules themselves, contributed to the effective drug encapsulation.[25,27] All DOX·HCl-loaded systems exhibited a negative surface charge around −30 to −40 mV (Figure 1B), indicating good dispersion stability,[39] which will also minimize the undesirable rapid elimination of DOX·HCl-loaded micellar NPs from the blood circulation, and facilitate their accumulation at the tumor sites.[29] There was an increase of zeta-potential, which was consistent with the consumption of the carboxylate groups by the drug molecules.

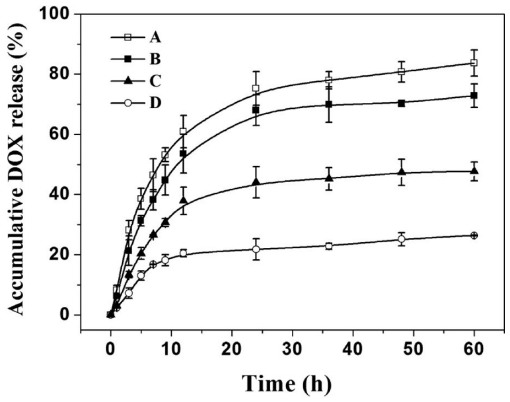

Figure 3. Time and pH-dependent DOX·HCl release profiles of DOX·HCl-loaded micellar NPs in (A) PBS at pH 5.5 with 10% FBS, (B) PBS at pH 5.5, (C) PBS at pH 7.4 with 10% FBS, and (D) PBS at pH 7.4. The data presented are means ± SD (n = 3).

A major concern in pharmaceutical industry consists in establishing convenient and reproducible methods to achieve high DLC and DLE. For this reason, the DOX·HCl-loaded nanoparticles with a polymer/DOX·HCl feed ratio of 5 (DLC = 16.1%, DLE = 96.7%) and 2 (DLC = 32.1%, DLE = 96.5%) were the ideal options. However, the DOX·HCl-loaded micellar NPs with polymer/DOX·HCl feed ratio of 2 had a hydrodynamic radius of 40−1000 nm with a broad distribution (see Figure S4 in the Supporting Information). The DOX·HCl-loaded nanoparticles with a lower DLC (16.1%) provided a significant better protection of the drug, showing a decreased drug release rate at physiological pH (see Figure S5 in the Supporting Information), which might actually contribute to a longer circulation in the bloodstream. Consequently, the DOX·HCl-loaded mPEG-*b*-PLG with a polymer/DOX·HCl feed ratio of 5 was applied for the following study. It was shown that the DOX·HCl-loaded micellar NPs had an average hydrodynamic radius of ∼90 nm with a narrow distribution (Figure 2), which might be an optimal size for the tumor targeting by the enhanced permeability and retention (EPR) effect.[40] Transmission electron microscopy image showed their spherical nanostructures (Figure 2). The smaller size (average radius around ∼65 nm) from TEM observation should be due to the dehydration of the micellar NPs in the TEM sample preparation process.[18]

In vitro Release of DOX·HCl. The in vitro release profiles of DOX·HCl-loaded mPEG-*b*-PLG were evaluated in different buffers (pH 5.5 with 10% FBS, pH 5.5, pH 7.4 and pH 7.4 with

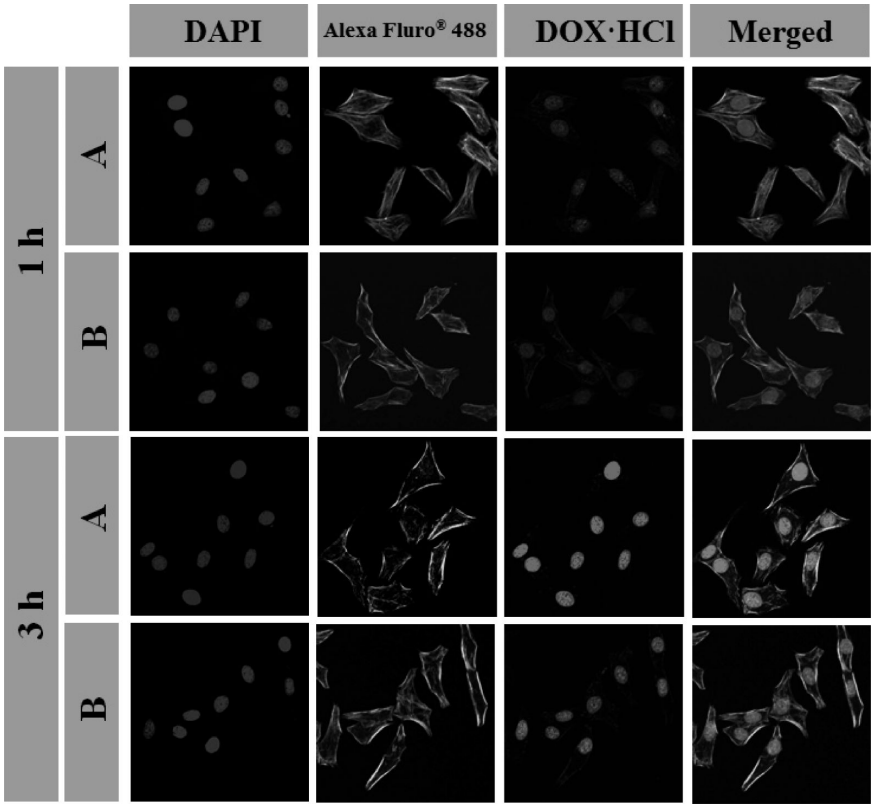

Figure 4. Cellular uptake of (A) free DOX·HCl and (B) mPEG-*b*-PLG-DOX·HCl after incubation with A549 cells for 1 and 3 h.

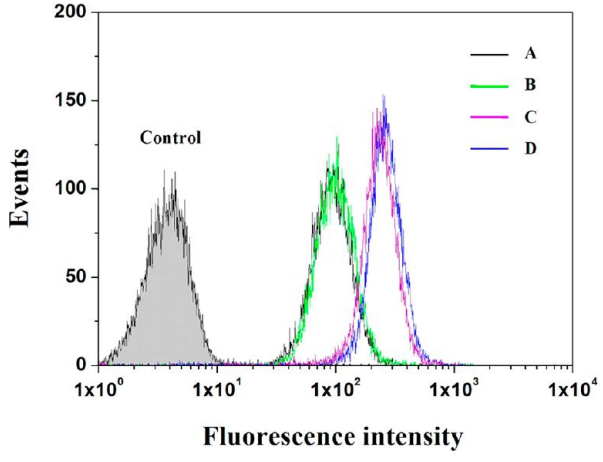

Figure 5. Fluorescent activated cell sorting analysis of cellular uptake of free DOX·HCl and mPEG-*b*-PLG-DOX·HCl after incubation with A549 cells for 1 and 3 h. (A) mPEG-*b*-PLG-DOX·HCl, 1 h; (B) free DOX·HCl, 1 h; (C) mPEG-*b*-PLG-DOX·HCl, 3 h and (D) free DOX·HCl, 3 h.

10% FBS) at 37 °C by dialysis method. As shown in Figure 3, under four releasing conditions, the release profile of DOX·HCl from DOX·HCl-loaded mPEG-*b*-PLG displayed a biphasic pattern that was characterized by a first rapid release followed by a slower and sustained release. After a 60 h incubation period, about 83.6, 72.8, 47.6, and 26.4% of DOX·HCl were released from mPEG-*b*-PLG-DOX·HCl in PBS at pH 5.5 with 10% FBS, PBS at pH 5.5, PBS at pH 7.4 with 10% FBS, and PBS at pH 7.4, respectively. DOX·HCl was released much more rapidly in pH 5.5 than in pH 7.4 PBS, which might be attributed to a significant reduction in the ionization degree of

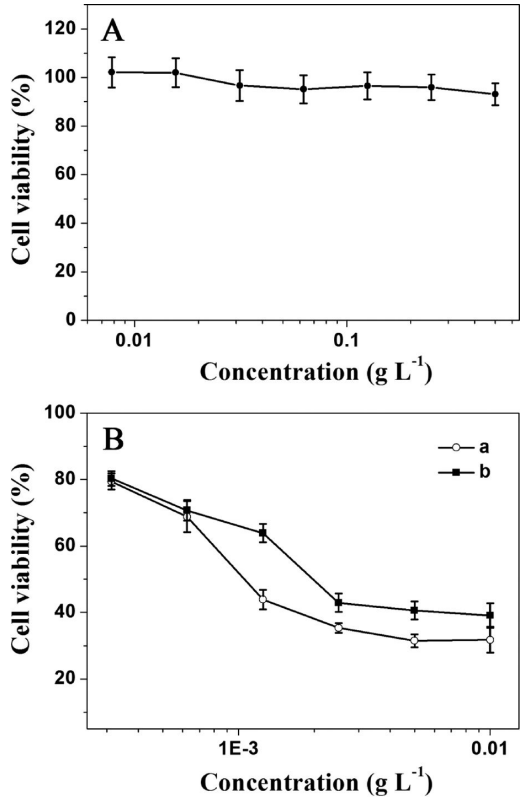

Figure 6. (A) In vitro cytotoxicity of mPEG-*b*-PLG against A549 cells; (B) cytotoxicities of (a) free DOX·HCl and (b) mPEG-*b*-PLG-DOX·HCl toward A549 cells.

dx.doi.org/10.1021/am303073u | *ACS Appl. Mater. Interfaces* 2013, 5, 1781−1792

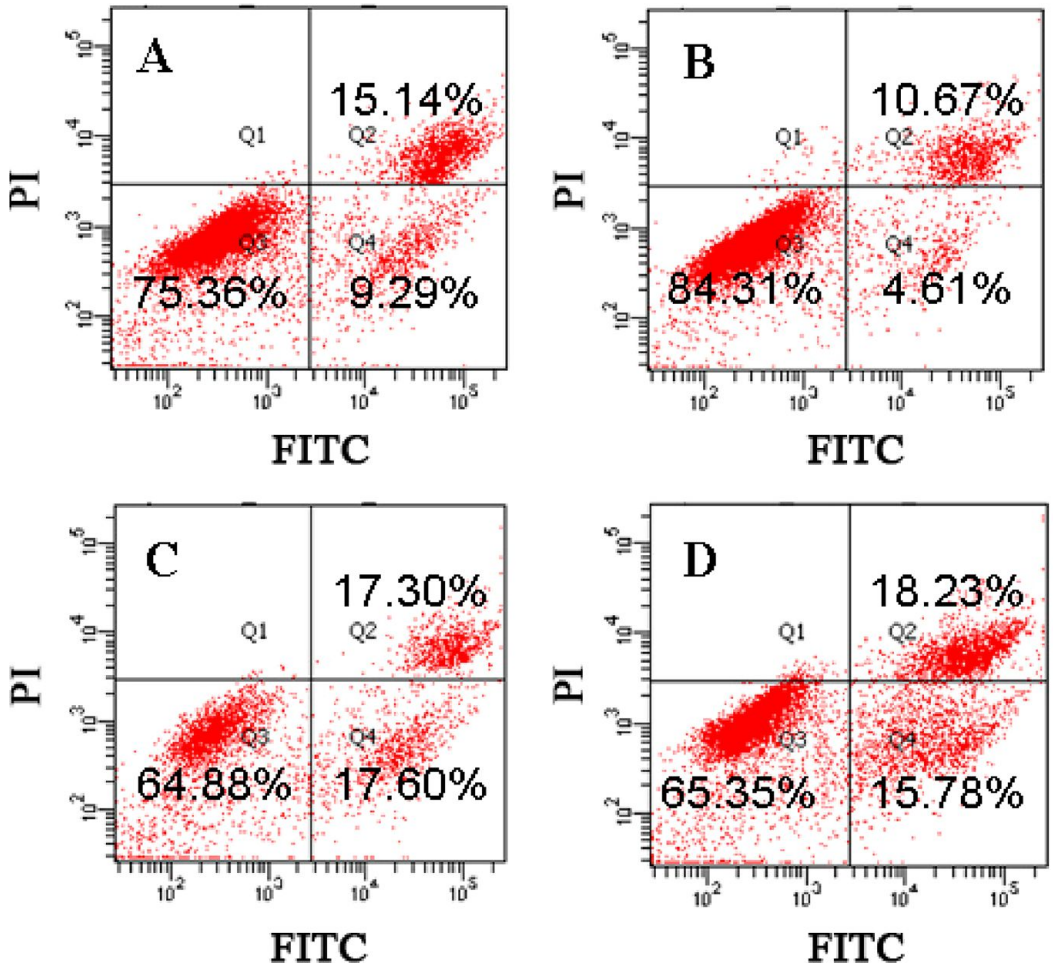

Figure 7. Apoptotic cell populations determined by flow cytometric analysis with Annexin V-FITC and propidium iodide (PI) staining after incubating A549 cells in DMEM media, with (A) free DOX·HCl for 4 h; (B) mPEG-*b*-PLG-DOX·HCl for 4 h; (C) free DOX·HCl for 24 h; and (D) mPEG-*b*-PLG-DOX·HCl for 24 h. The lower-left and upper-left quadrants in each panel indicate the populations of normal cells and necrotic cells, respectively, whereas the lower-right and upper-right quadrants in each panel indicate the populations of early and late apoptotic cells, respectively.

PLG moieties, resulting in extensive disruption of their electrostatic interactions with DOX·HCl.[25] In addition, increased hydrophilicity of DOX·HCl in acid condition also resulted in a rapid release of DOX·HCl.[27] Such a pH-triggered release behavior of DOX·HCl from mPEG-*b*-PLG-DOX·HCl showed great potential in drug delivery for the antiproliferative effect, due to the release of DOX·HCl in cells (Scheme 1) while limiting its release in blood circulation.[41] In vitro tests were also carried out in 10% FBS to better simulate the in vivo situation than with normal buffers. The increased release rate in 10% FBS suggested that FBS might facilitate this release because of the presence of enzymes in the serum.[41,42]

Cellular Uptake. To investigate the cellular internalization and intracellular release of DOX·HCl, we incubated mPEG-*b*-PLG-DOX·HCl with A549 cells for 1 and 3 h at 37 °C. The cells were then observed by confocal laser scanning microscopy. The cellular nuclei and cytoskeleton of A549 cells were selectively stained with DAPI (blue) and Alexa Fluor 488 (green), respectively. Red fluorescence imaging was performed to visualize the released DOX·HCl (Figure 4).

After 1 h incubation with free DOX·HCl and mPEG-*b*-PLG-DOX·HCl, the DOX·HCl fluorescence was both found to be aggregated in the cytosol and nuclei in both samples, whereas the DOX·HCl fluorescence intensity of mPEG-*b*-PLG-DOX·HCl observed in nuclei was slightly weaker than that of free DOX·HCl. When the incubation period increased to 3 h, DOX·HCl had mostly released into the perinuclei and nuclei region of cells. It should be noted that stronger DOX·HCl fluorescence was observed in cells following incubation with free DOX·HCl for 1 and 3 h, compared with the mPEG-*b*-PLG-DOX·HCl group. The lower DOX·HCl fluorescence observed for cells treated with mPEG-*b*-PLG-DOX·HCl than those with free DOX·HCl was most likely due to poor cellular uptake of mPEG-*b*-PLG-DOX·HCl that were stealthed by a dense layer of PEG shells and slow drug release from the micellar NPs.[43] On the other hand, the drug-loaded NPs exhibited negative surface charge, which would repel the anionic glycoproteins on the cell surface, and subsequently prevent cellular uptake.[44−46] For further confirmation, cellular uptake of DOX·HCl and mPEG-*b*-PLG-DOX·HCl into the A549 cells were analyzed using fluorescence-activated flow cytometry (Figure 5), and the consistent results were acquired.

Endocytosis, a general entry mechanism for macromolecules, is an ATP (adenosine triphosphate)-dependent process, which is attenuated down at low temperatures.[47] To assess whether the DOX·HCl-loaded micellar NPs enter cells via endocytosis, we incubated cells with FITC-labeled mPEG-*b*-PLG-DOX·HCl and compared the fluorescence accumulation to cells at 4 and 37 °C via confocal laser scanning microscopy analysis. Incubation of A549 cells with FITC-labeled mPEG-*b*-PLG-

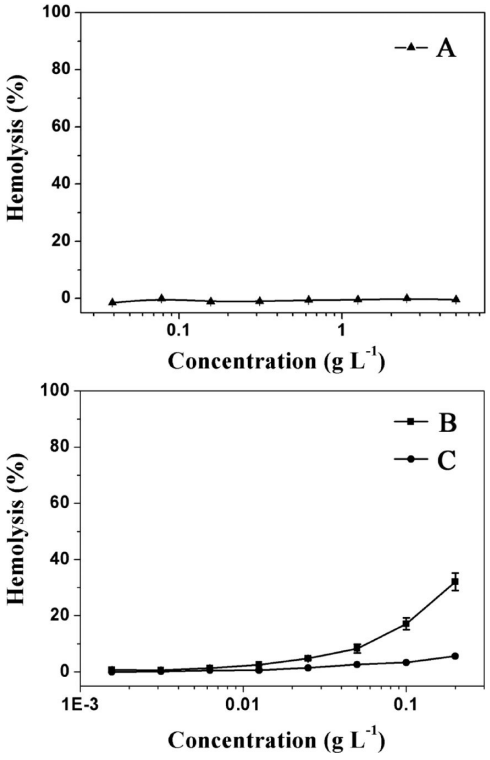

Figure 8. Hemolytic activity of (A) mPEG-*b*-PLG, (B) free DOX·HCl, and (C) mPEG-*b*-PLG-DOX·HCl on rabbit red blood cells.

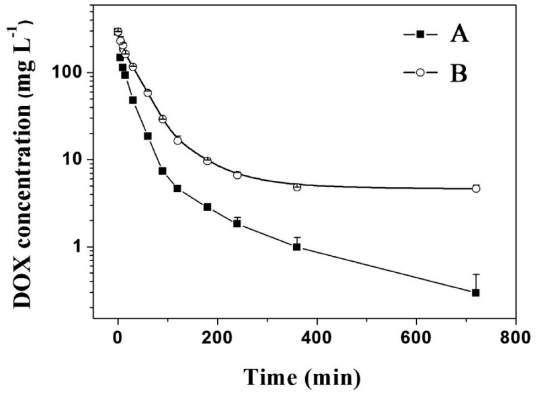

Figure 9. In vivo pharmacokinetics profiles after intravenous injection of (A) free DOX·HCl and (B) mPEG-*b*-PLG-DOX·HCl in rats. Points represent the means ± SD (n = 3).

Table 1. Pharmacokinetic Parameters of Free DOX·HCl and DOX·HCl-Loaded Micellar Nanoparticles

parameters	free DOX·HCl	mPEG-*b*-PLG-DOX·HCl
$t_{1/2}$ (min)	171.6 ± 28.3	237.6 ± 35.1
$AUC_{0\text{-}t}$ (mg min L^{-1})	5757.6 ± 695.0	16390.8 ± 1563.5
$AUC_{0\text{-}\infty}$ (mg min L^{-1})	5829.6 ± 851.7	16581.0 ± 1697.6
$MRT_{0\text{-}t}$ (min)	56.4 ± 10.6	121.8 ± 15.2
$MRT_{0\text{-}\infty}$ (min)	67.8 ± 13.5	130.8 ± 14.9
CL (mL min^{-1} kg^{-1})	51.45 ± 8.63	18.09 ± 4.21

DOX·HCl at 37 °C resulted in a time-dependent internalization of the drug-loaded NPs (see Figure S6 in the Supporting Information). In contrast, treatment at lower temperature, which interferes with endocytosis, resulted in a decrease in cellular uptake of FITC-labeled mPEG-*b*-PLG-DOX·HCl as shown in confocal microscope images (see Figure S6 in the Supporting Information), suggesting that mPEG-*b*-PLG-DOX·HCl was taken up by A549 cells via endocytosis.[21]

In vitro Cytotoxicity and Apoptotic Activity. The cytotoxicities of mPEG-*b*-PLG, free DOX·HCl, and mPEG-*b*-PLG-DOX·HCl against A549 cells were illustrated in Figure 6 by MTT assays. The block copolypeptide mPEG-*b*-PLG was found relatively nontoxic to the cells (cell viabilities: 93.1–102.1%) at concentrations of 7.8125 to 500 mg L^{-1}, indicating that mPEG-*b*-PLG micelles possessed excellent biocompatibility.

At an equivalent drug concentration, mPEG-*b*-PLG-DOX·HCl revealed a slightly lower antitumor activity as compared to free DOX·HCl, which agreed well with the intracellular DOX·HCl release observations (Figure 4), and was most probably because of the slightly slower uptake of mPEG-*b*-PLG-DOX·HCl and drug release from the micellar NPs.[43] Similar results were obtained in MCF-7 (see Figure S7 in the Supporting Information) and Hela cells (see Figure S8 in the Supporting Information), indicating its broad-spectrum anticancer activity.

Further, the death mechanisms of A549 cells treated with free DOX·HCl and mPEG-*b*-PLG-DOX·HCl for different time periods were evaluated by flow cytometry. Cells were double stained for viability (negative for propidium iodide (PI)) and apoptosis (positive for Annexin V-FITC). Incubated with the cells at a concentration of 1 μg mL^{-1} DOX·HCl-equivalent for 4 h, the mPEG-*b*-PLG-DOX·HCl and free DOX·HCl resulted in 4.61 and 9.29% early apoptotic cells, and 84.31 and 75.36% normal cells, respectively (Figure 7). However, a higher ratio of early apoptotic cells (15.78 and 17.60%) and lower ratio of normal cells (65.35 and 64.88%) were observed for both the mPEG-*b*-PLG-DOX·HCl and free DOX·HCl after a 24-h incubation time. The mPEG-*b*-PLG-DOX·HCl induced lower apoptosis than free DOX·HCl at the first 4 h, but this gap was narrowed during a prolonged incubation time. Taking into account the CLSM and in vitro drug release results, this could be ascribed to the comparably slower internalization and drug release from the carrier. This was further confirmed by FACS analysis (see Figure S9 in the Supporting Information).

Hemolysis. It is necessary to guarantee the blood compatibility of the drug-loaded nanocomposite, because it will be finally injected intravenously into blood vessels. In this study, a hemolysis assay was carried out based on the previous report.[32,38] As shown in the Figure 8A and Figure S10A (in the Supporting Information), mPEG-*b*-PLG showed negligible hemolysis toxicity (~0%) to RBCs even at the highest polymer concentration of 5 g L^{-1}, demonstrating the excellent blood compatibility of mPEG-*b*-PLG. Meanwhile, mPEG-*b*-PLG-DOX·HCl could significantly decrease the hemolysis of the RBCs compared to free DOX·HCl (Figure 8B, C and Figure S10B, C in the Supporting Information). The low and even negligible hemolytic activity should be originated from the outmost PEG shell serving as a protective layer, and the negatively charged surface.[48] These results indicated that DOX·HCl-loaded mPEG-*b*-PLG micellar NPs were hemocompatible, allowing the potential application as drug delivery vehicles.

Pharmacokinetics. Plasma pharmacokinetics of free DOX·HCl and mPEG-*b*-PLG-DOX·HCl formulations were evaluated with HPLC from plasma after intravenous administration. Plasma DOX·HCl concentration was the highest at the completion of injection and slowly decreased thereafter

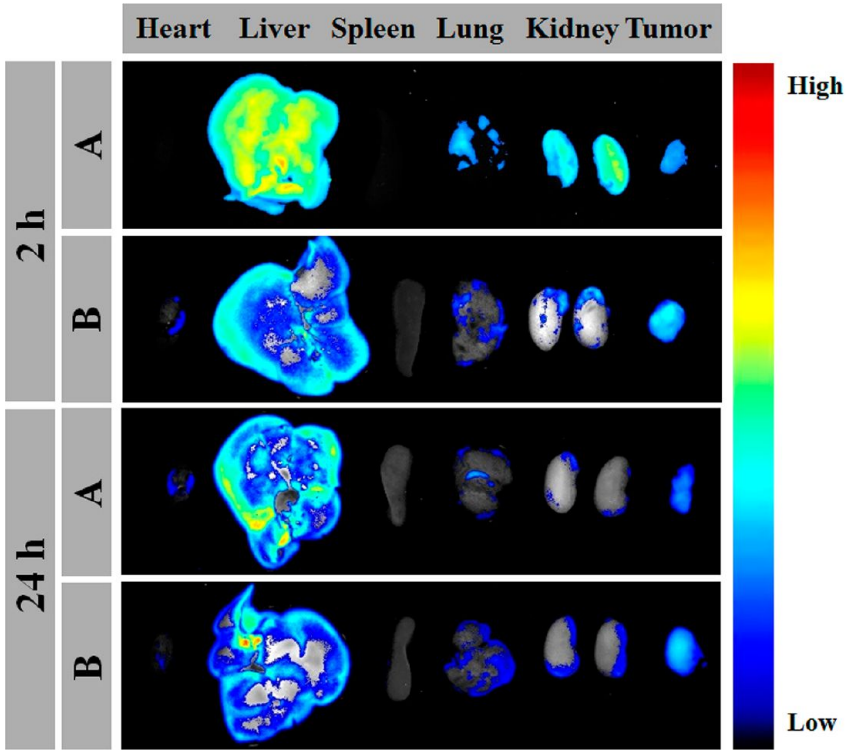

Figure 10. Ex vivo DOX·HCl fluorescence images showing the drug biodistribution of (A) free DOX·HCl and (B) mPEG-*b*-PLG-DOX·HCl in nude mice bearing A549 tumor at 2 and 24 h postinjection.

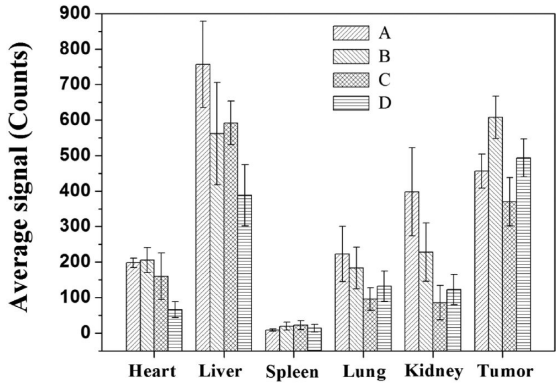

Figure 11. Average signals collected from the major organs (heart, liver, spleen, , and kidney) and tumor in nude mice bearing A549 tumor at different time points. (A) free DOX·HCl, 2 h; (B) mPEG-*b*-PLG-DOX·HCl, 2 h; (C) free DOX·HCl, 24 h; and (D) mPEG-*b*-PLG-DOX·HCl, 24 h.

(Figure 9). The blood circulation time of mPEG-*b*-PLG-DOX·HCl was significantly extended compared to free DOX·HCl (Figure 9 and Table 1), with a 1.4 times longer $t_{1/2}$, 2.2 times MRT_{0-t}, 2.8 times higher area under the curve (AUC_{0-t}), and substantially lower values for clearance, which may promote accumulation in tumor through the EPR effect. The decreased clearance of DOX·HCl in plasma in the mPEG-*b*-PLG-based nanoparticle group compared with the free DOX·HCl group might be explained by the in vitro sustained drug release (shown in Figure 3) and in vivo enhanced circulation of nanoparticles based on the PEGylated nanosized delivery vehicles.

Ex vivo DOX·HCl Fluorescence Imaging. For biodistribution studies, imaging of the isolated visceral organs (heart, liver, spleen, lung, kidney) and tumors at 2 and 24 h postinjection were carried out in nude mice bearing A549 tumor, and the results were shown in Figure 10. To semiquantitatively illustrate the biodistribution information, the photon numbers per unit area (average signals) of four different parts of the isolated visceral organs and tumors were collected and shown in Figure 11. At 2 h postinjection, liver and kidney showed strong DOX·HCl fluorescence for free DOX·HCl group, suggesting that drug molecules as foreign bodies were mainly captured and metabolized by liver and kidney.[49,50] However, fairly weaker fluorescence in both liver and kidney, and stronger fluorescence in tumor for the injection of mPEG-*b*-PLG-DOX·HCl were observed, indicating that the DOX·HCl-loaded mPEG-*b*-PLG micellar NPs were able to alter the biodistribution of the drug and contribute to reduce systemic toxicity. At 24 h postinjection, DOX·HCl fluorescence in tumor was slightly weakened as detected in ex vivo imaging, and meanwhile liver and kidney showed even much weaker fluorescence for both free DOX·HCl and mPEG-*b*-PLG-DOX·HCl formulations. However, a stronger fluorescence signal was also found in tumor administered by mPEG-*b*-PLG-DOX·HCl compared with that of free DOX·HCl. In accordance with the results received from the pharmacokinetics study (Figure 9 and Table 1), mPEG-*b*-PLG-DOX·HCl showed less reticuloendothelial system (RES) uptake and more tumor accumulation than free DOX·HCl, which could contribute to increasing the cancer therapy efficiency.

In vivo Anticancer Efficacy. To examine in vivo antitumor efficacy, we treated Balb-c/nude mice bearing human lung tumors (A549) with PBS, free DOX·HCl, and mPEG-*b*-PLG-DOX·HCl. All the mice were alive during the experimental period. As shown in panels A and B in Figure 12, both free DOX·HCl and mPEG-*b*-PLG-DOX·HCl formulations were effective in retarding tumor growth compared to control

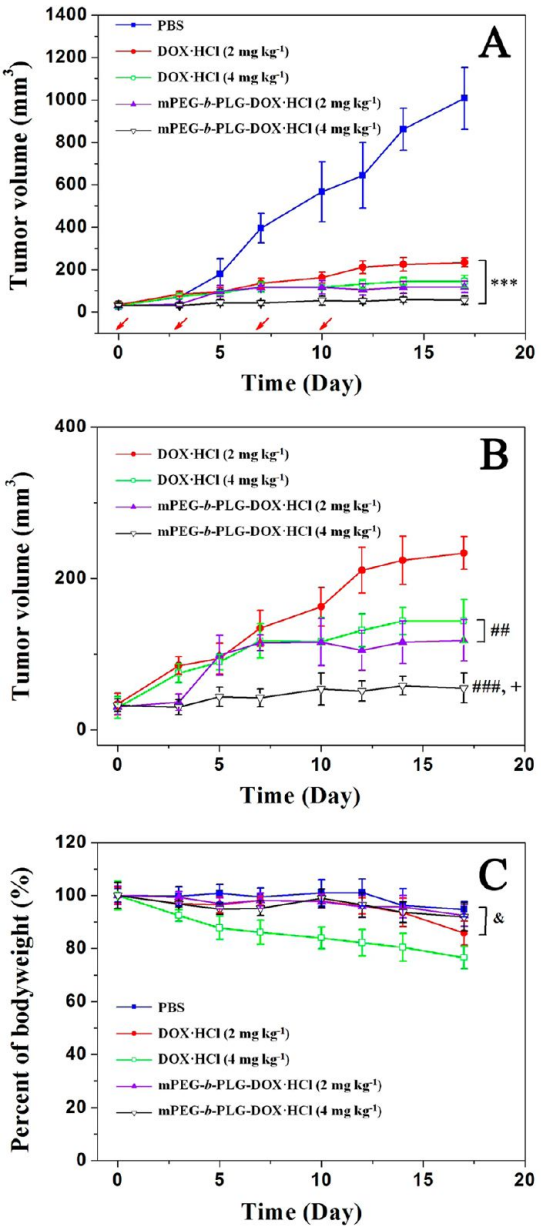

Figure 12. In vivo antitumor efficacy of various DOX·HCl formulations in the A549 tumor bearing mouse model. (A) Tumor sizes of the mice as a function of time; (B) amplificatory figure of tumor volume and (C) body weight changes with the time of tumor-bearing mice. The arrows represent the day on which the intravenous tail vein injection was performed. $^{***}p < 0.001$ versus PBS group. $^{\#\#}p < 0.01$ and $^{\#\#\#}p < 0.001$ versus free DOX·HCl (2 mg kg^{-1}) group. $^{+}p < 0.05$ versus mPEG-*b*-PLG-DOX·HCl (2 mg kg^{-1}) group. $^{\&}p < 0.05$ versus free DOX·HCl (4 mg kg^{-1}) group.

treatment with PBS. At day 17 postinjection, the average tumor volumes of free DOX·HCl (2 mg kg^{-1}), free DOX·HCl (4 mg kg^{-1}), mPEG-*b*-PLG-DOX·HCl (2 mg kg^{-1}) and mPEG-*b*-PLG-DOX·HCl (4 mg kg^{-1}) were 23.1, 14.2, 11.7, and 5.5% of that in the control group, respectively ($p < 0.001$), indicating a dose-dependent antitumor activity. The most efficient inhibition of tumor growth was observed in the mPEG-*b*-PLG-DOX·HCl treated group at a dose of 4 mg kg^{-1}. On the other hand, the average tumor volume of the group that received free DOX·HCl (2 mg kg^{-1}) was about 2.0-fold ($p < 0.01$) and 4.2-fold ($p < 0.001$), compared to that of the group received mPEG-*b*-PLG-DOX·HCl (2 mg kg^{-1}) and mPEG-*b*-PLG-DOX·HCl (4 mg kg^{-1}), respectively. Comparison between group d (mPEG-*b*-PLG-DOX·HCl, 2 mg kg^{-1}) and e (mPEG-*b*-PLG-DOX·HCl, 4 mg kg^{-1}) revealed obvious dose dependence of the tumor inhibition ($p < 0.05$). These results indicated that the mPEG-*b*-PLG-DOX·HCl inhibited tumor growth much more efficiently than free DOX·HCl formulation, and the group that received a 4 mg kg^{-1} DOX·HCl dose showed the most effective antitumor efficacy among the testing groups. The enhanced tumor inhibition of the mPEG-*b*-PLG-DOX·HCl might be mainly due to the prolonged circulation time and sustained DOX·HCl release in the tumor tissue after particle accumulation via the EPR effect.

Body weight loss is an important indicator to evaluate doxorubicin-induced toxicity. Figure 12C depicted body weight of the mice during the test. Mice treated with free DOX·HCl at a dose of 4 mg kg^{-1} exhibited a 24% decrease in body weight within 17 days, and appeared to be weak after treatment. Evident dose dependent systemic toxicity could be found, when group b (free DOX·HCl, 2 mg kg^{-1}) and c (free DOX·HCl, 4 mg kg^{-1}) were compared. Slightly increasing the dose of DOX·HCl would result in significant damage to animals. In all other groups, the lack of significant change in body weight during the 17-day observation period confirmed the lower systemic toxicity.

In summary, mPEG-*b*-PLG-DOX·HCl was an effective and safe enough drug formulation for the xenograft A549 cancer tumor model.

Histological and Immunohistochemical Analyses. To further evaluate antitumor efficacy after treatment with various formulations, we dissected the tumors from mice and sectioned for pathology analysis, after 17 days.

Tumor cells with a large nucleus and a spherical or spindle shape were observed in the tumor tissue treated with PBS group, in which more chromatin and binucleolates were also observed (Figure 13). However, various degree of tissue necrosis were observed in the free DOX·HCl and mPEG-*b*-PLG-DOX·HCl treated groups at 2 and 4 mg kg^{-1} doses. Chromatin was concentrated and distributed around the edge, and nuclei became pyknotic or absence. The necrosis area in the mPEG-*b*-PLG-DOX·HCl (4 mg kg^{-1}) group was the largest among the tested groups, while the free DOX·HCl and mPEG-*b*-PLG-DOX·HCl (2 mg kg^{-1}) groups displayed a lower necrotic level. The degree of pathological caryokinesis in the tumor was lowered and coagulation necrosis was enhanced as the DOX·HCl dose increased. At the same DOX·HCl dose, the damage to tumor tissues treated with mPEG-*b*-PLG-DOX·HCl was higher than that for those receiving free DOX·HCl.

The terminal deoxynucleotidyl ransferase-mediated dUTP nick-end labeling (TUNEL) assay further detected DNA fragmentation, a marker of late apoptosis, in nuclei of tumor cells. As shown in Figure 13, little apoptosis was detected in tumor tissues treated by PBS. However, all the DOX·HCl formulations administered groups were detected obvious cell apoptosis. In line with the H&E observation, treatment of DOX·HCl-loaded micellar NPs increased apoptosis compared with free DOX·HCl at the same dose, whereas treatment of mPEG-*b*-PLG-DOX·HCl at a dose of 4 mg kg^{-1} showed the highest degree of cell apoptosis in tumor tissue.

Poly-ADP-ribose polymerase (PARP), an abundant DNA-binding enzyme that detects and signals DNA strand breaks, is one of the essential substrates cleaved by both caspase-3 and −7.[51] The presence of cleaved PARP1 is one of the most used

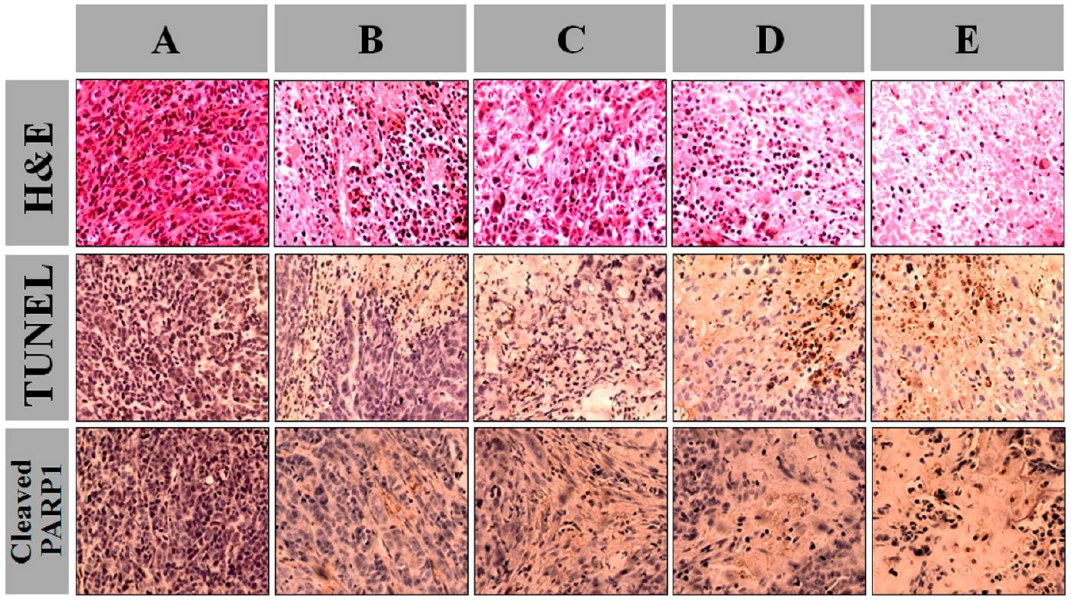

Figure 13. Ex vivo histological and immunohistochemical analyses of A549 tumor sections. (A) PBS; (B) free DOX·HCl (2 mg kg^{-1}); (C) free DOX·HCl (4 mg kg^{-1}); (D) mPEG-*b*-PLG-DOX·HCl (2 mg kg^{-1}) and (E) mPEG-*b*-PLG-DOX·HCl (4 mg kg^{-1}). Nuclei were stained bluish violet, whereas extracellular matrix and cytoplasm were stained pink in H&E staining. Brown and blue stains indicated apoptotic and normal cells, respectively, in TUNEL analysis. Brown and blue stains indicated cleaved PARP1 and nuclei, respectively, in immunohistochemical assay.

diagnostic tools for the detection of apoptosis in many cell types.[36,52] To further confirm the tumor apoptosis, the cleaved 25 kDa fragment of PARP1 was analyzed in the tumor sections by immunohistochemistry. The cleavage products were detected in the sections of tumor tissues treated with various DOX·HCl formulations. However, intensive positive signals increased in the mPEG-*b*-PLG-DOX·HCl (2 and 4 mg kg^{-1})-treated tumors compared with free DOX·HCl-treated ones, indicating that more cells underwent apoptosis in these groups (Figure 13).

Together, these results clearly indicated that mPEG-*b*-PLG-DOX·HCl provided a higher therapeutic efficacy compared with the free drug and mPEG-*b*-PLG-DOX·HCl at a high dose (4 mg kg^{-1}) exhibited the greatest therapeutic efficacy among all the treatment groups.

CONCLUSIONS

A polypeptide-based block ionomer complex formed by anionic mPEG-*b*-PLG and cationic anticancer drug DOX·HCl was developed for NSCLC treatment. The excellent hemocompatibility, cytocompatibility and drug loading capability of this copolypeptide rendered its potential for delivering bioactive substance via intravenous injection. CLSM and FACS studies confirmed that the FITC-labeled drug delivery NPs were taken up by A549 cells via endocytosis, with a slightly slower cellular internalization compared with free DOX·HCl. This ionomer complex could effectively protect the loaded DOX·HCl molecules, significantly prolong the circulation time, and increase DOX·HCl accumulation in tumors compared with that of free DOX·HCl. The in vivo study using a human NSCLC xenograft tumor model demonstrated lower toxicity and higher antitumor efficacy of mPEG-*b*-PLG-DOX·HCl compared to free DOX·HCl at an equivalent drug dose. With convenient fabrication, favorable hemocompatibility and cytocompatibility, excellent drug loading and controlled release properties and prolonged circulation time, the pH responsive polypeptide-based block ionomer complex held great potential for achieving an optimal therapeutic effect of the transported drugs in NSCLC treatment. Further studies to translate this encapsulation approach to other cationic drugs and other tumor models are in progress.

ASSOCIATED CONTENT

Supporting Information

Synthetic routes of mPEG-*b*-PLG. ^{1}H NMR spectra of mPEG-*b*-PBLG and mPEG-*b*-PLG. GPC traces of mPEG-*b*-PBLG and mPEG-*b*-PLG. DLS and TEM of mPEG-*b*-PLG-DOX·HCl (DLC = 32.1%) in aqueous solution. DOX·HCl release profiles of DOX·HCl-loaded micellar NPs (DLC = 16.1 and 32.1%) in PBS at pH 7.4. CLSM images of A549 cells treated with FITC-labeled mPEG-*b*-PLG-DOX·HCl at 4 and 37 °C for 1 and 3 h. In vitro cytotoxicity of mPEG-*b*-PLG, free DOX·HCl and mPEG-*b*-PLG-DOX·HCl against MCF-7 and Hela cells. The fluorescent activated cell sorting analysis of cellular uptake of free DOX·HCl (1 mg L^{-1}) and mPEG-*b*-PLG-DOX·HCl (1 mg L^{-1}) after incubation with A549 cells for 1, 3, and 24 h. Photographs of hemolysis of RBCs in the presence of mPEG-*b*-PLG, free DOX·HCl and mPEG-*b*-PLG-DOX·HCl. This material is available as a PDF free of charge via the Internet at http://pubs.acs.org/.

AUTHOR INFORMATION

Corresponding Author

*E-mail: honghua@jlu.edu.cn (H.H.); xschen@ciac.jl.cn (X.C.). Fax: +86 431 85262112; Tel: +86 431 85262112

Author Contributions

†M.L. and W.S. contributed equally to this work.

Notes

The authors declare no competing financial interest.

ACKNOWLEDGMENTS

This research was financially supported by National Natural Science Foundation of China (Projects 20904053, 51173184,

51233004, 51021003, and 21104076), Ministry of Science and Technology of China (International Cooperation and Communication Program 2011DFR51090).

REFERENCES

(1) Yang, Y.; Hu, Y. X.; Wang, Y. H.; Li, J.; Liu, F.; Huang, L. *Mol. Pharm.* **2012**, *9*, 2280−2289.
(2) Lv, P. P.; Wei, W.; Yue, H.; Yang, T. Y.; Wang, L. Y.; Ma, G. H. *Biomacromolecules* **2011**, *12*, 4230−4239.
(3) Siegel, R.; Naishadham, D.; Jemal, A. *CA Cancer J. Clin.* **2012**, *62*, 10−29.
(4) Akao, T.; Kimura, T.; Hirofuji, Y.-s.; Matsunaga, K.; Imayoshi, R.; Nagao, J.-i.; Cho, T.; Matsumoto, H.; Ohtono, S.; Ohno, J.; Taniguchi, K.; Kaminishi, H. *J. Drug Target.* **2010**, *18*, 550−556.
(5) Lalatsa, A.; Schatzlein, A. G.; Mazza, M.; Thi, B. H. L.; Uchegbu, I. F. *J. Controlled Release* **2012**, *161*, 523−536.
(6) Negishi, T.; Koizumi, F.; Uchino, H.; Kuroda, J.; Kawaguchi, T.; Naito, S.; Matsumura, Y. *Br. J. Cancer* **2006**, *95*, 601−606.
(7) Kataoka, K.; Matsumoto, T.; Yokoyama, M.; Okano, T.; Sakurai, Y.; Fukushima, S.; Okamoto, K.; Kwon, G. S. *J. Controlled Release* **2000**, *64*, 143−153.
(8) Adams, M. L.; Kwon, G. S. *J. Controlled Release* **2003**, *87*, 23−32.
(9) Wang, X.; Li, J.; Wang, Y.; Cho, K. J.; Kim, G.; Gjyrezi, A.; Koenig, L.; Giannakakou, P.; Shin, H. J. C.; Tighiouart, M.; Nie, S.; Chen, Z.; Shin, D. M. *ACS Nano* **2009**, *3*, 3165−3174.
(10) Bae, Y.; Nishiyama, N.; Fukushima, S.; Koyama, H.; Yasuhiro, M.; Kataoka, K. *Bioconjugate Chem.* **2005**, *16*, 122−130.
(11) Yu, S. F.; Wang, Z.; Wu, G. L.; Wang, Y. N.; Gao, H.; Ma, J. B. *Acta Polym. Sin.* **2012**, *4*, 427−432.
(12) Koizumi, F.; Kitagawa, M.; Negishi, T.; Onda, T.; Matsumoto, S.; Hamaguchi, T.; Matsumura, Y. *Cancer Res.* **2006**, *66*, 10048−10056.
(13) Harada, A.; Kataoka, K. *Macromolecules* **1998**, *31*, 288−294.
(14) Vachutinsky, Y.; Oba, M.; Miyata, K.; Hiki, S.; Kano, M. R.; Nishiyama, N.; Koyama, H.; Miyazono, K.; Kataoka, K. *J. Controlled Release* **2011**, *149*, 51−57.
(15) Nishiyama, N.; Okazaki, S.; Cabral, H.; Miyamoto, M.; Kato, Y.; Sugiyama, Y.; Nishio, K.; Matsumura, Y.; Kataoka, K. *Cancer Res.* **2003**, *63*, 8977−8983.
(16) Ding, D.; Wang, J.; Zhu, Z.; Li, R.; Wu, W.; Liu, B.; Jiang, X. *ACS Appl. Mater. Interfaces* **2012**, *4*, 1838−1846.
(17) Tyrrell, Z. L.; Shen, Y.; Radosz, M. *Prog. Polym. Sci.* **2010**, *35*, 1128−1143.
(18) Ding, J. X.; Shi, F. H.; Xiao, C. S.; Lin, L.; Chen, L.; He, C. L.; Zhuang, X. L.; Chen, X. S. *Polym. Chem.* **2011**, *2*, 2857−2864.
(19) Lee, S. J.; Min, K. H.; Lee, H. J.; Koo, A. N.; Rim, H. P.; Jeon, B. J.; Jeong, S. Y.; Heo, J. S.; Lee, S. C. *Biomacromolecules* **2011**, *12*, 1224−1233.
(20) Xu, Y.; Meng, F.; Cheng, R.; Zhong, Z. *Macromol. Biosci.* **2009**, *9*, 1254−1261.
(21) Cheng, Y.; Yu, S.; Zhen, X.; Wang, X.; Wu, W.; Jiang, X. *ACS Appl. Mater. Interfaces* **2012**, *4*, 5325−5332.
(22) Du, Y.; Chen, W.; Zheng, M.; Meng, F.; Zhong, Z. *Biomaterials* **2012**, *33*, 7291−7299.
(23) Song, Y. C.; Tong, W. J.; Gao, C. Y. *Acta Polym. Sin.* **2012**, *7*, 771−777.
(24) Nukolova, N. V.; Oberoi, H. S.; Cohen, S. M.; Kabanov, A. V.; Bronich, T. K. *Biomaterials* **2011**, *32*, 5417−5426.
(25) Huang, W.-C.; Chiang, W.-H.; Huang, Y.-F.; Lin, S.-C.; Shih, Z.-F.; Chern, C.-S.; Chiang, C.-S.; Chiu, H.-C. *J. Drug Target.* **2011**, *19*, 944−953.
(26) Manocha, B.; Margaritis, A. *J. Nanomater.* **2010**, *2010*, 1−9.
(27) Sanson, C.; Schatz, C.; Le Meins, J. F.; Soum, A.; Thevenot, J.; Garanger, E.; Lecommandoux, S. *J. Controlled Release* **2010**, *147*, 428−435.
(28) Al-Ahmady, Z. S.; Al-Jamal, W. T.; Bossche, J. V.; Bui, T. T.; Drake, A. F.; Mason, A. J.; Kostarelos, K. *ACS Nano* **2012**, *6*, 9335−9346.
(29) Xiao, K.; Li, Y.; Luo, J.; Lee, J. S.; Xiao, W.; Gonik, A. M.; Agarwal, R. G.; Lam, K. S. *Biomaterials* **2011**, *32*, 3435−3446.
(30) Tian, L.; Bae, Y. H. *Colloids Surf., B* **2012**, *99*, 116−126.
(31) Ding, J. X.; Zhuang, X. L.; Xiao, C. S.; Cheng, Y. L.; Zhao, L.; He, C. L.; Tang, Z. H.; Chen, X. S. *J. Mater.Chem.* **2011**, *21*, 11383−11391.
(32) Zhao, L.; Ding, J. X.; Xiao, C. S.; He, P.; Tang, Z. H.; Pang, X.; Zhuang, X. L.; Chen, X. S. *J. Mater. Chem.* **2012**, *22*, 12319−12328.
(33) Ernsting, M. J.; Tang, W. L.; MacCallum, N.; Li, S. D. *Bioconjugate Chem.* **2011**, *22*, 2474−2486.
(34) Shi, F.; Ding, J.; Xiao, C.; Zhuang, X.; He, C.; Chen, L.; Chen, X. *J. Mater. Chem.* **2012**, *22*, 14168−14179.
(35) Cho, H.-J.; Yoon, I.-S.; Yoon, H. Y.; Koo, H.; Jin, Y.-J.; Ko, S.-H.; Shim, J.-S.; Kim, K.; Kwon, I. C.; Kim, D.-D. *Biomaterials* **2012**, *33*, 1190−1200.
(36) Fu, C. L.; Lin, L.; Shi, H. L.; Zheng, D. X.; Wang, W.; Gao, S. Q.; Zhao, Y. F.; Tian, H. Y.; Zhu, X. J.; Chen, X. S. *Biomaterials* **2012**, *33*, 4589−4596.
(37) Dai, J.; Lin, S.; Cheng, D.; Zou, S.; Shuai, X. *Angew. Chem., Int. Ed.* **2011**, *50*, 9404−9408.
(38) Song, W.; Li, M.; Tang, Z.; Li, Q.; Yang, Y.; Liu, H.; Duan, T.; Hong, H.; Chen, X. *Macromol. Biosci.* **2012**, *12*, 1514−1523.
(39) Wang, Z.; Yu, Y.; Dai, W.; Lu, J.; Cui, J.; Wu, H.; Yuan, L.; Zhang, H.; Wang, X.; Wang, J.; Zhang, X.; Zhang, Q. *Biomaterials* **2012**, *33*, 8451−8460.
(40) Dufort, S.; Sancey, L.; Coll, J.-L. *Adv. Drug Delivery Rev.* **2012**, *64*, 179−189.
(41) Gao, H.; Qian, J.; Yang, Z.; Pang, Z.; Xi, Z.; Cao, S.; Wang, Y.; Pan, S.; Zhang, S.; Wang, W.; Jiang, X.; Zhang, Q. *Biomaterials* **2012**, *33*, 6264−6272.
(42) Zong, H.; Thomas, T. P.; Lee, K.-H.; Desai, A. M.; Li, M.-h.; Kotlyar, A.; Zhang, Y.; Leroueil, P. R.; Gam, J. J.; Banaszak Holl, M. M.; Baker, J. R. *Biomacromolecules* **2012**, *13*, 982−991.
(43) Wei, R.; Cheng, L.; Zheng, M.; Cheng, R.; Meng, F.; Deng, C.; Zhong, Z. *Biomacromolecules* **2012**, *13*, 2429−2438.
(44) Freese, C.; Gibson, M. I.; Klok, H.-A.; Unger, R. E.; Kirkpatrick, C. J. *Biomacromolecules* **2012**, *13*, 1533−1543.
(45) Perry, J. L.; Herlihy, K. P.; Napier, M. E.; Desimone, J. M. *Acc. Chem. Res.* **2011**, *44*, 990−998.
(46) Zhu, S.; Qian, L.; Hong, M.; Zhang, L.; Pei, Y.; Jiang, Y. *Adv. Mater.* **2011**, *23*, H84−H89.
(47) Lee, Y.; Graeser, R.; Kratz, F.; Geckeler, K. E. *Adv. Funct. Mater.* **2011**, *21*, 4211−4218.
(48) Xiao, Q.; Bu, W.; Ren, Q.; Zhang, S.; Xing, H.; Chen, F.; Li, M.; Zheng, X.; Hua, Y.; Zhou, L.; Peng, W.; Qu, H.; Wang, Z.; Zhao, K.; Shi, J. *Biomaterials* **2012**, *33*, 7530−7539.
(49) Ma, P. A.; Liu, S.; Huang, Y. B.; Chen, X. S.; Zhang, L. P.; Jing, X. B. *Biomaterials* **2010**, *31*, 2646−2654.
(50) Xing, T.; Mao, C.; Lai, B.; Yan, L. *ACS Appl. Mater. Interfaces* **2012**, *4*, 5662−5672.
(51) Bressenot, A.; Marchal, S.; Bezdetnaya, L.; Garrier, J.; Guillemin, F.; Plenat, F. *J. Histochem. Cytochem.* **2009**, *57*, 289−300.
(52) Misra, R.; Sahoo, S. K. *Mol. Pharm.* **2011**, *8*, 852−866.